VIP Sodium-Ion Batteries Very Important Paper

International Edition: DOI: 10.1002/anie.201713417
German Edition: DOI: 10.1002/ange.201713417

Reversible Redox Chemistry of Azo Compounds for Sodium-Ion Batteries

*Chao Luo, Gui-Liang Xu, Xiao Ji, Singyuk Hou, Long Chen, Fei Wang, Jianjun Jiang, Zonghai Chen, Yang Ren, Khalil Amine, and Chunsheng Wang**

Abstract: *Sustainable sodium-ion batteries (SSIBs) using renewable organic electrodes are promising alternatives to lithium-ion batteries for the large-scale renewable energy storage. However, the lack of high-performance anode material impedes the development of SSIBs. Herein, we report a new type of organic anode material based on azo group for SSIBs. Azobenzene-4,4′-dicarboxylic acid sodium salt is used as a model to investigate the electrochemical behaviors and reaction mechanism of azo compound. It exhibits a reversible capacity of 170 mAh g^{-1} at 0.2C. When current density is increased to 20C, the reversible capacities of 98 mAh g^{-1} can be retained for 2000 cycles, demonstrating excellent cycling stability and high rate capability. The detailed characterizations reveal that azo group acts as an electrochemical active site to reversibly bond with Na$^+$. The reversible redox chemistry between azo compound and Na ions offer opportunities for developing long-cycle-life and high-rate SSIBs.*

With the advent of renewable energy for smart grids, Li-ion batteries (LIBs), the dominant power supply for most portable electronics, cannot satisfy the vast demand from the market owing to the lack of lithium resources in the earth crust.[1,2] It is important to search for an inexpensive and abundant alternative to LIBs for the large-scale application of smart grids. Na-ion batteries (SIBs), which share similar chemistry to LIBs, are promising alternatives, because sodium is the sixth most abundant element in the earth. In the last decade, extensive research efforts were devoted to developing high performance SSIBs for large-scale renewable energy storage, and significant advance in high performance cathode materials (such as sodium metal oxides,[3–5] sodium metal phosphates,[6,7] sulfur[8,9] and selenium[10,11]) has been achieved. However, the lack of high-performance anode material limits the development of SIBs since the high performance LIB anodes (such as, graphite and silicon) are inactive for SIBs, while sodium metal suffers from safety issue induced by dendrite growth.[12] Although Na-ion can co-intercalate into graphite with diglyme at a low potential, its low specific capacity of less than 100 mAh g^{-1}, limits the energy density of SIBs.[13] Therefore, developing high performance renewable anode materials becomes a major challenge for SSIBs.

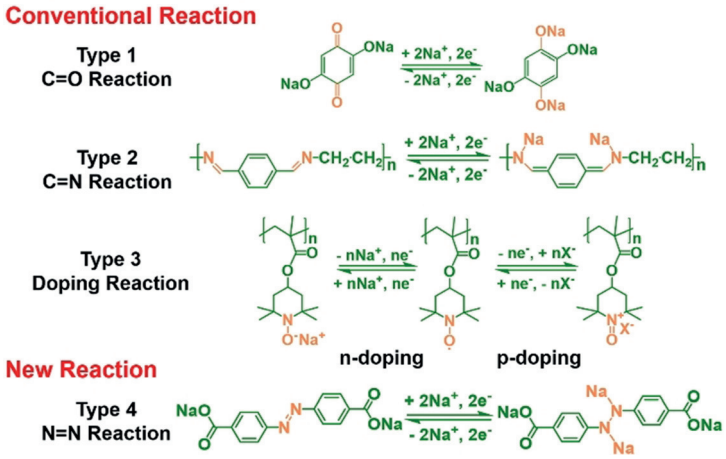

Scheme 1. Reaction mechanisms for organic electrode materials.

Organic compounds, which are abundant, inexpensive, sustainable and recyclable, are promising anode materials for SSIBs.[14–16] There are three categories of organic electrodes based on carbonyl (C=O), imine (C=N), and doping reactions in SIBs (Scheme 1).[17–21] The doping-reaction-based organic materials, such as organic radicals, display high reaction potentials during the p-doping process with anions (ClO_4^-, PF_6^-), and are not suitable for anodes, while the conventional organic anodes are mainly based on carbonyl and imine compounds, which provide carbonyl and imine redox centers to reversibly react with Na ions at relatively low reaction potentials.[22–25] The typical carbonyl compounds such as sodium terephthalate[26,27] and benzoquinone derivatives,[28,29] and imine compounds such as Schiff base derivatives[30] exhibit high specific capacity (> 150 mAh g^{-1}) in SIBs. How-

[*] Dr. C. Luo, X. Ji, S. Hou, Dr. L. Chen, Dr. F. Wang, Prof. C. Wang
Department of Chemical and Biomolecular Engineering, University of Maryland
College Park, MD 20740 (USA)
E-mail: cswang@umd.edu
Dr. G. Xu, Dr. Z. Chen, Dr. Y. Ren, Dr. K. Amine
Chemical Sciences and Engineering Division, Argonne National Laboratory
Argonne, IL 60439 (USA)
X. Ji, Prof. J. Jiang
School of Optical and Electronic Information, Huazhong University of Science and Technology
Wuhan, Hubei, 430074 (China)
Dr. K. Amine
IRMC, Imam Abdulrahman Bin Faisal University (IAU)
Dammam (Saudi Arabia)
Supporting information and the ORCID identification number(s) for the author(s) of this article can be found under: https://doi.org/10.1002/anie.201713417.

ever, the conventional organic anodes still suffer from low power density and short cycle life. Most organic materials cannot maintain high capacity at a current density over 20C and very rare organic material show a cycle life longer than 1000 cycles in SIBs. No organic compounds can satisfy the requirements of high power density and long cycle life for large-scale SSIBs.

Herein, we report a new type of organic electrode materials based on azo group (N=N) for large-scale SSIBs. The azo group can function as a redox center to reversibly react with Na-ions. Three organic compounds (Figure 1),

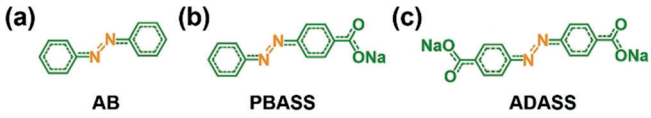

Figure 1. Molecular structure of a) AB, b) PBASS, and c) ADASS.

azobenzene (AB), 4-(phenylazo)benzoic acid sodium salt (PBASS), and azobenzene-4,4′-dicarboxylic acid sodium salt (ADASS), were selected as model azo compounds to evaluate their electrochemical performance in SIBs. AB is selected as a basic model aromatic azo compound since it contains only one functional azo group in the center. However, it has high solubility in the organic electrolyte as evidenced by Figure S1 in the Supporting Information. The colorless electrolyte becomes orange after mixing with AB. To suppress the dissolution of AB, carboxylate groups are added in AB to generate PBASS and ADASS. Among them, ADASS exhibits the best electrochemical performance, in terms of high-rate capability and long cycle life. ADASS provides 170 mAh g^{-1} at 0.2C, and retains 66% and 58% of the capacity when the current density increases to 10C and 20C, respectively. Moreover, a reversible capacity of 98 mAh g^{-1} is retained for 2000 cycles at 20C with a slow capacity decay rate of 0.0067% per cycle. The detailed characterizations using X-ray diffraction (XRD), Raman spectroscopy and density functional theory (DFT) calculations confirm azo group functions as an electrochemical active site to reversibly bond with Na ions as shown in Scheme 1. Therefore, azo compounds are a new category of anode materials for high performance SIBs.

The structure and morphology of PBASS and ADASS were characterized by XRD, Raman spectroscopy, Fourier-transform infrared spectroscopy (FTIR), thermal gravimetric analysis (TGA) and scanning electron microscopy (SEM). As shown in Figure S2–3, PBASS and ADASS have crystalline structures with typical Raman peaks for azo group in 1400–1450 cm^{-1} range,[31] and typical IR peaks for azo group in 1575–1630 cm^{-1} range.[32] In addition, they display increasing baseline intensity in Raman spectra (Figure S2b and S3b) owing to the fluorescence emitted by azo compounds. TGA results (Figure S2d, S3d) show PBASS and ADASS are stable up to 405 °C and 325 °C, respectively. The SEM images (Figure S2e, S3e) show that PBASS and ADASS consist of micro-sized particles. Therefore, chemical characterizations confirm the molecular structure and particle size of PBASS and ADASS.

The electrochemical performance of azo compounds was measured in coin cells with sodium metal as counter electrode. In Figure S4a, AB exhibits two long and flat plateaus at 2.0 V and 1.35 V with ultrahigh capacity of 929 mAh g^{-1} during the first discharge. However, the high solubility of AB in the electrolyte significantly reduces the corresponding charge capacity to 15 mAh g^{-1}. To reduce the solubility of AB, a carboxylate group is added into AB to form PBASS. As shown in Figure S4b, PBASS delivers two pairs of charge/discharge plateaus centered at 1.1 V and 1.4 V with discharge capacities approximately 162 mAh g^{-1}. However, the Coulombic efficiency of PBASS is about 115% in the charge/discharge cycling (Figure S4c), demonstrating that PBASS still dissolves into the electrolyte, resulting in a severe shuttle reaction. To further suppress the shuttle reaction, an additional carboxylate group is added to PBASS to form ADASS. As shown in Figure 2a, ADASS displays two flat plateaus at 1.2 V and 1.26 V during discharge and corresponding two charge plateaus at 1.37 V and 1.43 V, which are consistent with one broad cathodic peak at 1.2 V and two sharp anodic peaks at 1.37 V and 1.43 V in cyclic voltammetry (CV) scan (Figure 2b). The single cathodic peak at 1.2 V in CV scan demonstrates that two pairs of sodiation/de-sodiation peaks are close to each other and overlapped. Adding

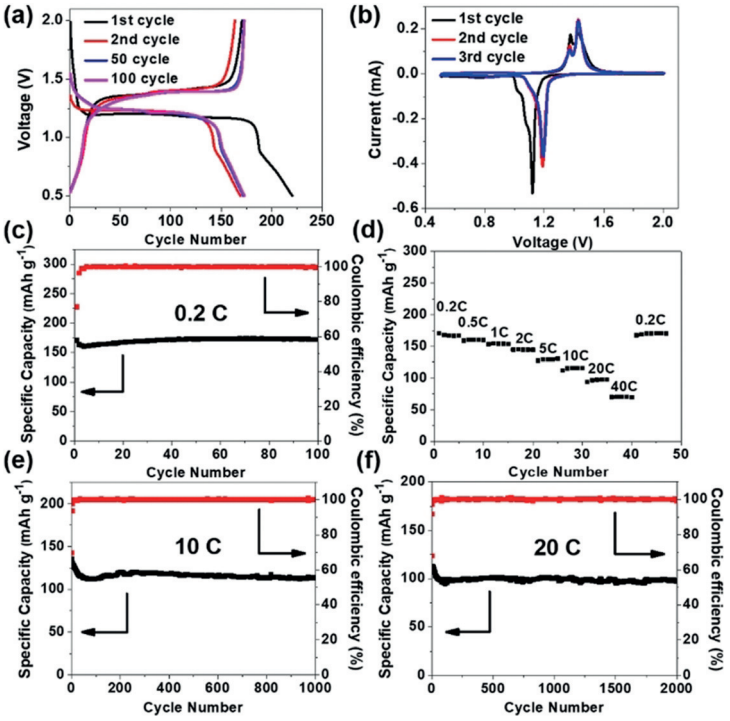

Figure 2. The electrochemical performance of ADASS in Na-ion batteries. a) The galvanostatic charge–discharge curves at 0.2C; b) Cyclic voltammograms at 0.1 mV s^{-1}; c) De-sodiation capacity and Coulombic efficiency versus cycle number at the current density of 0.2C; d) Rate performance at various C-rates; De-sodiation capacity and Coulombic efficiency versus cycle number at 10C (e) and 20C (f).

carboxylate group in azobenzene cannot only reduce the solubility, but also change the sodiation/desodiation potentials. The low solubility of ADASS in the electrolyte enables ADASS to stably charge/discharge for 100 cycles with Coulombic efficiency of approximately 100% even at a low rate of 0.2C (Figure 2c). Moreover, when the current density increases from 0.2C to 40C (Figure 2d), a reversible capacity of 71 mAh g^{-1} is retained, demonstrating the robust reaction kinetics. To further evaluate the long-term cycling stability, ADASS is cycled at 10C and 20C for 1000 cycles and 2000 cycles (Figure 2e,f), and ADASS retains reversible capacities of 113 mAh g^{-1} after 1000 cycles and 98 mAh g^{-1} after 2000 cycles, further confirming the high cycling stability and high-rate capability. Therefore, the exceptional electrochemical performance of ADASS manifests that azo compounds are promising anode materials for SIBs.

The mechanism for excellent electrochemical kinetics of ADASS was investigated using electrochemical impedance spectroscopy (EIS), galvanostatic intermittent titration technique (GITT) and CV. Figure S5 shows the EIS evolution of ADASS electrode upon cycling. The interphase resistance of pristine ADASS electrode, represented by the depressed semi-circle, is very small (ca. 20 Ohm), and only slightly increases to about 30 Ohm after 5 cycles owing to the formation of solid electrolyte interface (SEI) layer. The small interphase resistance enables the high-rate capability of ADASS electrode. GITT measurement was conducted to check the overpotential and equilibrium potential of ADASS upon cycling. As shown in Figure 3a–c, the quasi-equilibrium potential in the first three charge/discharge cycles is stable (Figure 3c). However, the overpotential of ADASS during the first discharge is larger than the subsequent charge/discharge cycles as a result of large strain/stress in the pristine ADASS (Figure 3a–c). After the first discharge, the overpotential of ADASS at the charge/discharge plateaus is small (ca. 0.03 V) and stable, coincident with the small interphase resistance in Figure S5. The equilibrium potentials obtained from GITT in Figure 3d show that the charge/discharge equilibrium potentials of ADASS is at 1.37 V/1.25 V, and the potential hysteresis is only 0.12 V. The small overpotential and potential hysteresis validate the high-rate capability of ADASS electrode. The reaction kinetics was further studied using CV at various scan rates (Figure 3e). With elevated scan rate, the cathodic peaks shift to lower potential, while the anodic peaks shift to higher potential, ascribing to the enhanced polarization. The linear fit of natural logarithm ln relationship of peak current and scan rate (Figure 3f) displays that the slopes of anodic and cathodic peaks are close to 0.5, demonstrating the reaction kinetics of ADASS is determined by Na-ion diffusion.[33] The extended π-conjugated structure in ADASS and strong Na^+ adsorption by nitrogen in azo group contribute to the fast Na-ion diffusion.[34] Therefore, the small interphase resistance/overpotential/potential hysteresis and fast Na-ion diffusion result in the high-rate capability of ADASS.

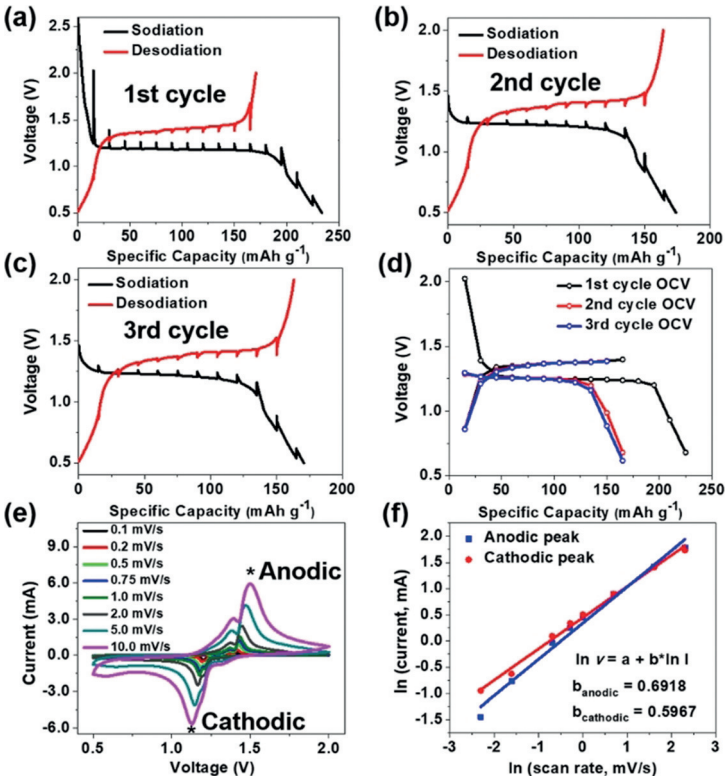

Figure 3. Potential response of ADASS electrode in the a) first cycle, b) second cycle, c) third cycle during GITT measurements; d) Equilibrium potential versus specific capacity during GITT measurement OCV = open circuit potential; e) CV curves of ADASS at various scan rates; f) The ln relationship of peak current and scan rate for ADASS.

The phase and structure change of ADASS during sodiation/desodiation were investigated using XRD, Raman spectroscopy and DFT calculations. As shown in the in situ XRD patterns (Figure 4a), during the discharge from 2.5 V to 0.5 V, the typical XRD peaks of ADASS at 16.6°, 17.3° and 18.2° gradually decrease, while two new peaks at 19° and 22° appear after ADASS is sodiated to below 1.2 V, demonstrating the formation of a new phase at 1.2 V. The color-map clearly shows that the red and yellow areas for XRD peaks of pristine ADASS become very weak after ADASS is discharged from 2.5 V to 1.2 V, while the new yellow areas in Figure 4a for XRD peaks at 19° and 22° show up at 1.2 V and become stronger from 1.2 V to 0.5 V, confirming the phase transformation during initial sodiation. Figure 4b shows the XRD patterns of the pristine ADASS and fully charged ADASS electrodes after 5 cycles. The fully recovered XRD peaks of cycled ADASS demonstrate excellent phase reversibility of ADASS in SIBs. In the Raman spectra (Figure 4c), when ADASS is fully discharged to 0.5 V, the characteristic Raman peak at 1450 cm^{-1} for azo group disappears. Instead, a new peak at 1295 cm^{-1}, representing the sodiated azo group (Na-N-N-Na), appears, demonstrating the azo group reacts with Na ions during the sodiation process. When ADASS electrode is charged to 2 V, the characteristic Raman peak at 1450 cm^{-1} for azo group recovers, demonstrating reversible electrochemical reaction between azo group and Na ions. Additionally, the Raman peak at 1600 cm^{-1} for carbonyl

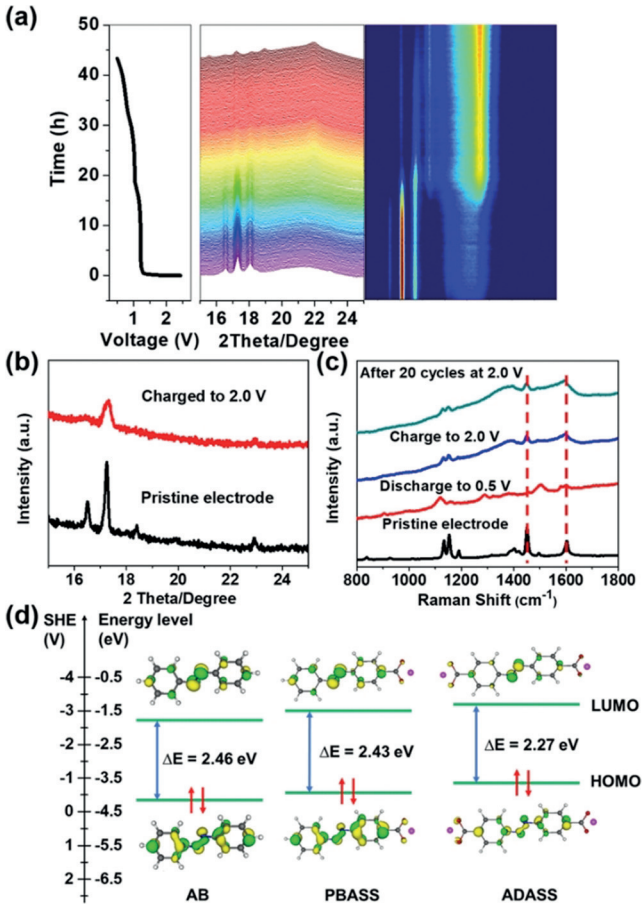

Figure 4. a) In situ synchrotron XRD patterns and color-mapped profile of ADASS electrode, and the corresponding voltage profile; b) XRD spectra of ADASS electrodes before and after 5 cycles; c) Raman spectra of ADASS electrodes before and after 5 cycles and 20 cycles, broken vertical lines indicate Raman peaks for azo and carboxylate groups; d) DFT calculation results for the relative energies and optimized structures of AB, PBASS, and ADASS (The right axis aligns the relative energies in vacuum to the relative potential versus the standard hydrogen electrode (SHE)).

group in ADASS does not change upon cycling, indicating carbonyl group does not participate in the reaction with Na ions. The reaction mechanism of azo compounds was further confirmed using DFT calculations. The energy levels of the lowest unoccupied molecular orbital (LUMO) and the highest occupied molecular orbital (HOMO) for AB, PBASS, and ADASS are visualized in Figure 4d. The charge density isosurfaces of LUMO states for AB, PBASS, and ADASS demonstrate that the electron localizes in the azo group during sodiation, confirming azo group is the electrochemical active site for the reduction of azo compound. Therefore, the detailed characterizations and DFT calculations confirm that azo group is the electrochemical active site to reversibly react with Na ions.

In summary, azo compounds, a new family of organic active materials, are reported as anode materials in SIBs. An aromatic azo compound, ADASS, is employed as a model to investigate the electrochemical performance, reaction kinetics and mechanism of azo compound. ADASS delivers a reversible capacity of 170 mAh g^{-1} at 0.2C, and retains the reversible capacities of 113 mAh g^{-1} and 98 mAh g^{-1} at 10C and 20C for 1000 cycles and 2000 cycles, respectively, demonstrating exceptional cycling stability and rate capability. The detailed characterizations and DFT calculations unravel that the small interphase resistance and low potential hysteresis contribute to the high rate capability, and the azo group in ADASS acts as an electrochemical active site to reversibly bond with Na ions. Therefore, azo compounds as a new family of organic electrode materials are promising for developing long-cycle-life and high-rate SSIBs.

Acknowledgements

This work was supported by the US National Science Foundation award No.: 1438198. We acknowledge the support of the Maryland NanoCenter and its NispLab. The NispLab is supported in part by the NSF as a MRSEC Shared Experimental Facility.

Conflict of interest

The authors declare no conflict of interest.

Keywords: anodes · azo compounds · organic electrode materials · sodium-ion batteries

How to cite: *Angew. Chem. Int. Ed.* **2018**, *57*, 2879–2883
Angew. Chem. **2018**, *130*, 2929–2933

[1] H. Pan, Y.-S. Hu, L. Chen, *Energy Environ. Sci.* **2013**, *6*, 2338–2360.
[2] V. Palomares, P. Serras, I. Villaluenga, K. B. Hueso, J. Carretero-González, T. Rojo, *Energy Environ. Sci.* **2012**, *5*, 5884–5901.
[3] N. Yabuuchi, M. Kajiyama, J. Iwatate, H. Nishikawa, S. Hitomi, R. Okuyama, R. Usui, Y. Yamada, S. Komaba, *Nat. Mater.* **2012**, *11*, 512–517.
[4] M. Guignard, C. Didier, J. Darriet, P. Bordet, E. Elkaïm, C. Delmas, *Nat. Mater.* **2013**, *12*, 74–80.
[5] J. Billaud, G. Singh, A. R. Armstrong, E. Gonzalo, V. Roddatis, M. Armand, T. Rojo, P. G. Bruce, *Energy Environ. Sci.* **2014**, *7*, 1387–1391.
[6] A. Langrock, Y. Xu, Y. Liu, S. Ehrman, A. Manivannan, C. Wang, *J. Power Sources* **2013**, *223*, 62–67.
[7] Y. Zhu, Y. Xu, Y. Liu, C. Luo, C. Wang, *Nanoscale* **2013**, *5*, 780–787.
[8] X. Lu, B. W. Kirby, W. Xu, G. Li, J. Y. Kim, J. P. Lemmon, V. L. Sprenkle, Z. Yang, *Energy Environ. Sci.* **2013**, *6*, 299–306.
[9] S. Xin, Y. X. Yin, Y. G. Guo, L. J. Wan, *Adv. Mater.* **2014**, *26*, 1261–1265.
[10] A. Abouimrane, D. Dambournet, K. W. Chapman, P. J. Chupas, W. Weng, K. Amine, *J. Am. Chem. Soc.* **2012**, *134*, 4505–4508.
[11] C. Luo, Y. Xu, Y. Zhu, Y. Liu, S. Zheng, Y. Liu, A. Langrock, C. Wang, *ACS Nano* **2013**, *7*, 8003–8010.
[12] Z. W. Seh, J. Sun, Y. Sun, Y. Cui, *ACS Cent. Sci.* **2015**, *1*, 449–455.
[13] B. Jache, P. Adelhelm, *Angew. Chem. Int. Ed.* **2014**, *53*, 10169–10173; *Angew. Chem.* **2014**, *126*, 10333–10337.
[14] T. B. Schon, B. T. McAllister, P.-F. Li, D. S. Seferos, *Chem. Soc. Rev.* **2016**, *45*, 6345–6404.

[15] Y. Xu, M. Zhou, Y. Lei, *Mater. Today* **2017**, https://doi.org/10.1016/j.mattod.2017.07.005.
[16] M. Lee, J. Hong, J. Lopez, Y. Sun, D. Feng, K. Lim, W. C. Chueh, M. F. Toney, Y. Cui, Z. Bao, *Nat. Energy* **2017**, *2*, 861 – 868.
[17] Q. Zhao, Y. Lu, J. Chen, *Adv. Energy Mater.* **2017**, *7*, 1601792.
[18] Q. Zhao, J. Wang, Y. Lu, Y. Li, G. Liang, J. Chen, *Angew. Chem. Int. Ed.* **2016**, *55*, 12528 – 12532; *Angew. Chem.* **2016**, *128*, 12716 – 12720.
[19] C. Luo, X. Fan, Z. Ma, T. Gao, C. Wang, *Chem* **2017**, *3*, 1050 – 1062.
[20] M. Lee, J. Hong, D. H. Seo, D. H. Nam, K. T. Nam, K. Kang, C. B. Park, *Angew. Chem. Int. Ed.* **2013**, *52*, 8322 – 8328; *Angew. Chem.* **2013**, *125*, 8480 – 8486.
[21] J. Hong, M. Lee, B. Lee, D.-H. Seo, C. B. Park, K. Kang, *Nat. Commun.* **2014**, *5*, 5335.
[22] C. Luo, Y. Zhu, Y. Xu, Y. Liu, T. Gao, J. Wang, C. Wang, *J. Power Sources* **2014**, *250*, 372 – 378.
[23] H. Padhy, Y. Chen, J. Lüder, S. R. Gajella, S. Manzhos, P. Balaya, *Adv. Energy Mater.* **2017**, DOI: https://doi.org/10.1002/aenm.201701572.
[24] S. Wang, L. Wang, Z. Zhu, Z. Hu, Q. Zhao, J. Chen, *Angew. Chem. Int. Ed.* **2014**, *53*, 5892 – 5896; *Angew. Chem.* **2014**, *126*, 6002 – 6006.
[25] E. Castillo-Martínez, J. Carretero-González, M. Armand, *Angew. Chem. Int. Ed.* **2014**, *53*, 5341 – 5345; *Angew. Chem.* **2014**, *126*, 5445 – 5449.
[26] Y. Park, D. S. Shin, S. H. Woo, N. S. Choi, K. H. Shin, S. M. Oh, K. T. Lee, S. Y. Hong, *Adv. Mater.* **2012**, *24*, 3562 – 3567.
[27] L. Zhao, J. Zhao, Y. S. Hu, H. Li, Z. Zhou, M. Armand, L. Chen, *Adv. Energy Mater.* **2012**, *2*, 962 – 965.
[28] C. Luo, J. Wang, X. Fan, Y. Zhu, F. Han, L. Suo, C. Wang, *Nano Energy* **2015**, *13*, 537 – 545.
[29] W. Luo, M. Allen, V. Raju, X. Ji, *Adv. Energy Mater.* **2014**, *4*, 1400554.
[30] M. López-Herraiz, E. Castillo-Martínez, J. Carretero-González, J. Carrasco, T. Rojo, M. Armand, *Energy Environ. Sci.* **2015**, *8*, 3233 – 3241.
[31] M. M. J. Tecklenburg, D. J. Kosnak, A. Bhatnagar, D. K. Mohanty, *J. Raman Spectrosc.* **1997**, *28*, 755 – 763.
[32] I. A. Mohammed, A. Mohammed, *Molecules* **2010**, *15*, 7498 – 7508.
[33] V. Augustyn, J. Come, M. A. Lowe, J. W. Kim, P.-L. Taberna, S. H. Tolbert, H. D. Abruña, P. Simon, B. Dunn, *Nat. Mater.* **2013**, *12*, 518 – 522.
[34] C. Wang, Y. Xu, Y. Fang, M. Zhou, L. Liang, S. Singh, H. Zhao, A. Schober, Y. Lei, *J. Am. Chem. Soc.* **2015**, *137*, 3124 – 3130.

Manuscript received: December 31, 2017
Version of record online: February 9, 2018

